Journal of Non-Newtonian Fluid Mechanics 259 (2018) 125–129

Contents lists available at ScienceDirect

Journal of Non-Newtonian Fluid Mechanics

journal homepage: www.elsevier.com/locate/jnnfm

Short Communication

Effect of the solvent viscosity on pure electro-osmotic flow of viscoelastic fluids

L.L. Ferrás[b,c], A.S. Cavadas[d], P.R. Resende[e], A.M. Afonso[a,*], F.T. Pinho[a]

[a] Centro de Estudos de Fenómenos de Transporte, Departamento de Engenharia Mecânica, Faculdade de Engenharia da Universidade do Porto, Rua Dr. Roberto Frias s/n Porto, 4200-465, Portugal
[b] Centro de Matemática - UM, Departamento de Matemática, Universidade do Minho Guimarães, 4800-058, Portugal
[c] Institute for Polymers and Composites/I3N, University of Minho, Campus de Azurém Guimarães, 4800-058, Portugal
[d] Departamento de Engenharia Mecânica, Faculdade de Engenharia da Universidade do Porto, Rua Dr. Roberto Frias s/n Porto, 4200-465, Portugal
[e] Universidade Estadual Paulista (Unesp), Instituto de Ciência e Tecnologia, Sorocaba, Brasil

ARTICLE INFO

Keywords:
Electro-osmosis
Viscoelastic fluids
Newtonian solvent

ABSTRACT

In this work the fully-developed steady channel flow of the homogeneous polymer solution studied in [4] is revisited and a completely new analytical solution is proposed which is devoid of the limitations of the previous solution ($\beta^3 \varepsilon De_\kappa^2 \leq 2/27$), i.e., it is valid for the complete range of the rheological parameters. The viscoelastic fluid is described by the simplified Phan–Thien and Tanner model with linear stress coefficient function for the polymer contribution plus a Newtonian solvent. The solution is also valid if the polymer contribution is described by the finitely extensive non-linear elastic model with the Peterlin approximation for the average spring force (FENE-P model).

1. Introduction

Forcing motion in microchannels through the application of an external electric field (electro osmotic flow - EOF) on fluids of complex rheology, many of which are engineered for specific applications, is becoming more common. Of particular interest are viscoelastic fluids, and even though their components may interact in a complex manner with the electric fields and surfaces, leading either to adsorption or wall-depletion, as described in the specialized literature [1,5,6], we are concerned here with the simple fully-developed steady channel flow of homogeneous polymer solutions described by the simplified Phan–Thien and Tanner model with linear stress coefficient function for the polymer contribution plus a Newtonian solvent. This problem is of interest, for instance, to verify numerical methods in more complex situations and it was in this context that this flow was previously addressed in the appendix of Afonso et al. [4], where an analytical solution was originally proposed, but subject to constraints that limited its range of application, such as $\beta^3 \varepsilon De_\kappa^2 \leq 2/27$. In this short communication we present a completely new analytical solution devoid of such restrictions and then briefly discuss the effects of the solvent to polymer viscosity ratio and viscoelasticity upon the flow characteristics, since such an analysis is missing from the literature.

2. Analytical solution

We consider microfluidic transport of a viscoelastic fluid through a parallel plate microchannel (see Fig. 1) of height $2H$, length L and width w, with $w \gg 2H$. The origin of the coordinate system is at the symmetry plane. An electric potential gradient is applied along the axis of the channel, which provides the necessary driving force for the flow. At the wall the no-slip condition applies and at the centreplane flow symmetry conditions apply (flow symmetry conditions are anti-symmetry of the shear stress, hence $\tau_{xy} = 0$ at $y = 0$), so only one half of the channel ($0 < y < H$) is considered for mathematical analysis (both walls are identical). To obtain a closed form solution for the velocity distribution, some simplifying assumptions are introduced: steady and fully developed flow, i.e. $u = u(y)$, $v = 0$; no overlap of the spontaneously formed wall electric double layers, and validity of the Debye–Hückel linearization principle. Based on these assumptions the governing equations reduce to (for more details see the original work [4])

$$\nabla \cdot \boldsymbol{\tau} = -\rho_e \mathbf{E} + \nabla p - \eta_s \nabla^2 \cdot \mathbf{u}, \tag{1}$$

$$f\left(\boldsymbol{\tau}_{kk}\right)\boldsymbol{\tau} + \lambda \overset{\nabla}{\boldsymbol{\tau}} = 2\eta_p \mathbf{D}, \tag{2}$$

$$\nabla \cdot (\nabla \psi) = -\frac{\rho_e}{\epsilon}. \tag{3}$$

* Corresponding author.
E-mail addresses: luis.ferras@dep.uminho.pt (L.L. Ferrás), adelioc@fe.up.pt (A.S. Cavadas), resende@sorocaba.unesp.br (P.R. Resende), aafonso@fe.up.pt (A.M. Afonso), fpinho@fe.up.pt (F.T. Pinho).

https://doi.org/10.1016/j.jnnfm.2018.04.008
Received 21 September 2017; Accepted 24 April 2018
Available online 27 April 2018

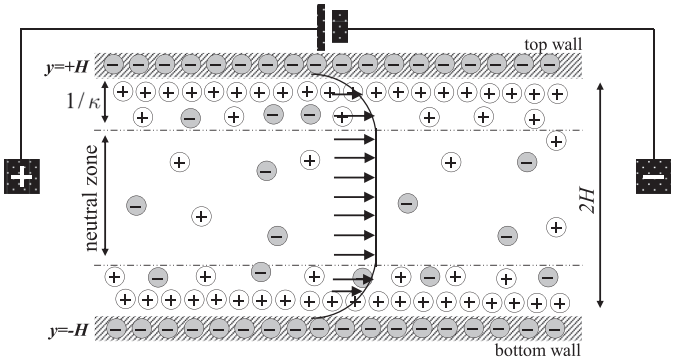

Fig. 1. Schematic of the flow in a parallel plate microchannel. The case represented is for a fluid-wall combination leading to a negative charge at the wall.

$$\rho_e = -2n_o ez \sinh\left(\frac{ez}{k_B T}\psi\right), \tag{4}$$

In the momentum equation (Eq. (1)) $\mathbf{u}$ is the velocity vector, p the pressure, t the time, η_s the Newtonian solvent viscosity, $\boldsymbol{\tau}$ the polymeric extra stress contribution, $\mathbf{E}$ is the applied external electric field and ρ_e is the net electric charge density. The constitutive model adopted here to represent the polymer contribution is the simplified PTT model (Phan—Thien and Tanner [7,8]), and can be expressed by Eq. (2) where $\mathbf{D}$ is the rate of deformation tensor, λ the relaxation time, η_p the polymeric viscosity and $\overset{\nabla}{\boldsymbol{\tau}}$ represents the upper convected time derivative defined as $\overset{\nabla}{\boldsymbol{\tau}} = \frac{D\boldsymbol{\tau}}{Dt} - (\nabla\mathbf{u})^T \cdot \boldsymbol{\tau} - \boldsymbol{\tau} \cdot \nabla\mathbf{u}$. The stress coefficient function, $f(\boldsymbol{\tau}_{kk})$ can be expressed in the linearised form, given by $f(\boldsymbol{\tau}_{kk}) = 1 + \frac{\epsilon\lambda}{\eta_p}\boldsymbol{\tau}_{kk}$, where ϵ represents the extensibility parameter and $\boldsymbol{\tau}_{kk}$ is the trace of tensor $\boldsymbol{\tau}$.

Eq. (3)is the equation for the potential field within the electric double layer (EDL) expressed by means of a Poisson–Boltzmann equation. Here, ψ denotes the EDL potential and ϵ is the dielectric constant of the solution. The net electric charge density, ρ_e, is described by Eq. (4) where n_o is the ion density, e is the electronic charge, z the valence of the ions, k_B Boltzmann's constant, and T is the absolute temperature.

This system of equation can be further simplified to give the following momentum equation,

$$\frac{d\tau_{xy}^p}{dy} = -\rho_e E_x - \eta_s \frac{d^2u}{dy^2}. \tag{5}$$

The superscript p is from now on used to refer to the polymer contribution ($\boldsymbol{\tau}$ in Eqs. (1) and (2)), to better distinguish from the solvent contribution. The net charge density distribution, Eq. (4), can also be obtained, being given by:

$$\rho_e = -\epsilon\kappa^2 \frac{\zeta_0 \cosh(\kappa y)}{\cosh(\kappa H)} \tag{6}$$

where $\kappa^2 = \frac{2n_o e^2 z^2}{\epsilon k_B T}$ is the Debye–Hückel parameter, related with the thickness of the Debye layer, $\xi = \frac{1}{\kappa}$ (normally referred to as the EDL thickness). This approximation is valid when the Debye thickness is small but finite, i.e., for $10 \lesssim H/\xi \lesssim 10^3$. Also, the following relation between the streamwise normal stress and shear stress is obtained,

$$\tau_{xx} = 2\frac{\lambda}{\eta_p}\tau_{xy}^2. \tag{7}$$

Using Eq. (6) and considering symmetry ($\tau_{xy\|y=0} = 0$), Eq. (5) can be integrated to yield

$$\tau_{xy}^p = \epsilon\zeta_0 E_x \kappa \frac{\sinh(\kappa y)}{\cosh(\kappa H)} - \eta_s \frac{du}{dy}. \tag{8}$$

Using Eq. (7), an explicit expression for the polymer normal stress component is obtained,

$$\tau_{xx}^p = 2\frac{\lambda}{\eta_p}\left(\epsilon\zeta_0 E_x \kappa \frac{\sinh(\kappa y)}{\cosh(\kappa H)} - \eta_s \frac{du}{dy}\right)^2. \tag{9}$$

Note that Eq. (9) is consistent with the required boundary condition at the centerline, i.e. $\tau_{xx\|y=0} = 0$. From the simplification of Eq. (1) (see [4]), we obtain

$$\left(1 + 2\frac{\varepsilon\lambda^2}{\eta_p^2}\left(\tau_{xy}^p\right)^2\right)\tau_{xy}^p = \eta_p \frac{du}{dy} = \frac{\eta_p}{\eta_s}\left(-\tau_{xy}^p + \epsilon\zeta_0 E_x \kappa \frac{\sinh(\kappa y)}{\cosh(\kappa H)}\right). \tag{10}$$

For the last equality on the right-hand side, the integrated momentum Eq. (8) was expressed explicitly in terms of the local shear rate du/dy. After rearranging the various terms in Eq. (10) we arrive at the following cubic equation for the polymer shear stress

$$\left(\tau_{xy}^p\right)^3 + \frac{\eta_p^2}{2\varepsilon\lambda^2}\left(\frac{\eta_s + \eta_p}{\eta_s}\right)\tau_{xy}^p - \frac{\eta_p^2}{2\varepsilon\lambda^2}\left(\epsilon\zeta_0 E_x \kappa \frac{\eta_p}{\eta_s}\frac{\sinh(\kappa y)}{\cosh(\kappa H)}\right) = 0, \tag{11}$$

where β represents the viscosity ratio, $\frac{\eta_s}{\eta_s+\eta_p}$. One may also think of $1-\beta$ as a quantity proportional to the polymer concentration. The solution of this cubic equation is given in classical books as

$$\tau_{xy}^p = \sqrt[3]{-\frac{b}{2} + \sqrt{\frac{b^2}{4} + \frac{a^3}{27}}} + \sqrt[3]{-\frac{b}{2} - \sqrt{\frac{b^2}{4} + \frac{a^3}{27}}} \tag{12}$$

$$a = \frac{\eta_p^2}{2\beta\varepsilon\lambda^2}; b = -\frac{\eta_p^2}{2\varepsilon\lambda^2}\left(\frac{1-\beta}{\beta}\right)\epsilon\zeta_0 E_x \kappa \frac{\sinh(\kappa y)}{\cosh(\kappa H)} \tag{13}$$

In dimensionless form, the shear and normal stresses are given by:

$$\bar{\tau}_{xy}^p = \sqrt[3]{-\bar{b} + \sqrt{\bar{b}^2 + \frac{\bar{a}^3}{27}}} + \sqrt[3]{-\bar{b} - \sqrt{\bar{b}^2 + \frac{\bar{a}^3}{27}}}$$
$$\bar{a} = \frac{\bar{\kappa}^2(1-\beta)^2}{2\beta^3\varepsilon De_\kappa^2}; \bar{b} = \frac{a(1-\beta)}{2}\frac{\bar{\kappa}\sinh(\bar{\kappa}\,\bar{y})}{\cosh(\bar{\kappa})} \tag{14}$$

$$\bar{\tau}_{xy}^p = \frac{2\beta De_\kappa}{\bar{\kappa}(1-\beta)}\bar{\tau}_{xy}^2 \tag{15}$$

respectively, where $\bar{y} = y/H$, $\bar{\kappa} = \kappa H$, $De_\kappa = \frac{\lambda u_{sh}}{\xi} = \lambda\kappa u_{sh}$ is the Deborah number based on the EDL thickness and on the Helmholtz–Smoluchowski electro-osmotic velocity, defined as $u_{sh} = -\frac{\epsilon\zeta_o E_x}{\eta_s}$ [9], and, $\bar{\tau}_{xy}^p = \frac{\tau_{xy}^p H}{u_{sh}\eta_s}$. The use of the Newtonian solvent viscosity coefficient to define the Helmholtz–Smoluchowski velocity and for normalization of the velocity profile is different from the previous works. The relationship between the Helmholtz–Smoluchowski velocities based on the solvent and polymeric part is $u_{sh} = \beta u_{sh}^p$. It should be remarked that we are obtaining the polymeric stresses depending on the solvent through β.

Going back to the momentum Eq. (8), we can re-write it as an equation for the dimensionless shear rate:

$$\frac{d\bar{u}}{d\bar{y}} = -\bar{\tau}_{xy}^p - \bar{\kappa}\frac{\sinh(\bar{\kappa}\,\bar{y})}{\cosh(\bar{\kappa})} \tag{16}$$

In order to integrate Eq. (16), we assume the following variable transformation and approximation, $\bar{\varphi} = \sinh(\bar{\kappa}\,\bar{y}) \approx \frac{1}{2}\exp(\bar{\kappa}\,\bar{y}) - \frac{1}{2}$, but still it will be assessed in the next section. This approximation is usually accurate as in many practical applications the finite electric double layer thickness is very small, about 1–3 orders of magnitude smaller than the thickness of the microfluidic channel [3,4]. Note that in the previous works [3,4] the approximation used was $\sinh(\bar{\kappa}\,\bar{y}) \approx \frac{1}{2}\exp(\bar{\kappa}\,\bar{y})$. The new approximation proved to be more accurate, avoiding at the same time the break of symmetry, reported in [3,4]. With $\bar{\varphi} \approx \frac{1}{2}\exp(\bar{\kappa}\,\bar{y}) - \frac{1}{2}$, we have that:

$$\int \frac{d\bar{u}}{d\bar{y}}\,d\bar{y} \approx \int \left(-\bar{\tau}_{xy\phi}^p - \frac{\bar{\kappa}\bar{\varphi}}{\cosh(\bar{\kappa})}\right)\frac{1}{\bar{\kappa}} ln\left(2\bar{\varphi} + 1\right)d\varphi \tag{17}$$

where $\overline{\tau}^{p}_{xy\phi}$ is the shear stress of Eq. (14) with $\bar{b} = \frac{a(1-\beta)}{2}\frac{\overline{\kappa}\varphi}{\cosh(\overline{\kappa})}$. If the integration is subject to the no-slip boundary condition at the wall ($\overline{u}_{\|\overline{\varphi}_{wall}} = 0$), the resulting velocity profile is (now using again the inverse approximation $\overline{\varphi} = \sinh(\overline{\kappa}\,\overline{y}) \approx \frac{1}{2}\exp(\overline{\kappa}\,\overline{y}) - \frac{1}{2}$),

$$\begin{aligned}\overline{u}(\overline{y}) = {} & \frac{1}{2}\mathrm{sech}(\overline{\kappa})\left(\log\left(\frac{2\sinh(\overline{\kappa}\,\overline{y})+1}{2\sinh(\overline{\kappa})+1}\right)\right. \\ & \left. -\,2\sinh(\overline{\kappa}\,\overline{y}) + 2\sinh(\overline{\kappa})\right) \\ & +\left(F^{-}(\overline{y}) - F^{-}(1) + F^{+}(\overline{y}) - F^{+}(1)\right) \end{aligned} \tag{18}$$

where $\overline{A} = \frac{\overline{\kappa}\left((1-\beta)^3\overline{\kappa}^2\right)}{(2\cosh(\overline{\kappa}))\left(2\beta^3\epsilon De_k^2\right)}$ and $\overline{B} = \frac{1}{27}\left(\frac{(1-\beta)^2\overline{\kappa}^2}{2\beta^3\epsilon De_k^2}\right)^3$ are constant parameters, and,

$$\Omega^{\pm}(\overline{y}) = \sqrt[3]{\overline{A}\sinh(\overline{\kappa}\,\overline{y}) \pm \sqrt{\overline{A}^2\sinh(\overline{\kappa}\,\overline{y})^2 + \overline{B}}} \tag{19}$$

$$\begin{aligned} F^{\pm}(\overline{y}) = {} & \frac{1}{2^{2/3}\sqrt{\theta\overline{\kappa}}} \\ & \left\{ 3 - \frac{\alpha\log\left(\sqrt[3]{-\frac{1}{2}}\sqrt[3]{\vartheta} + \Omega^{\pm}\right)}{\vartheta^{2/3}} - \frac{\alpha\log\left(\Omega^{\pm} - \frac{\sqrt[3]{\vartheta}}{\sqrt[3]{2}}\right)}{\vartheta^{2/3}} \right. \\ & - \frac{\left(-\overline{A}^2 + \overline{A}\sqrt{\theta} - 4\overline{B}\right)\log\left(\sqrt[3]{-\frac{1}{2}}\sqrt[3]{\sqrt{\theta}-\overline{A}} + \Omega^{\pm}\right)}{\left(\sqrt{\theta}-\overline{A}\right)^{2/3}} \\ & - \frac{\alpha\log\left(\frac{1}{2}\left(2\Omega^{\pm} - (-2)^{2/3}\sqrt[3]{\vartheta}\right)\right)}{\vartheta^{2/3}} \\ & - \frac{\left(-\overline{A}^2 + \overline{A}\sqrt{\theta} - 4\overline{B}\right)\log\left(\Omega^{\pm} - \frac{\sqrt[3]{\sqrt{\theta}-\overline{A}}}{\sqrt[3]{2}}\right)}{\left(\sqrt{\theta}-\overline{A}\right)^{2/3}} \\ & \left. - \frac{\left(-\overline{A}^2 + \overline{A}\sqrt{\theta} - 4\overline{B}\right)\log\left(\frac{1}{2}\left(2\Omega^{\pm} - (-2)^{2/3}\sqrt[3]{\sqrt{\theta}-\overline{A}}\right)\right)}{\left(\sqrt{\theta}-\overline{A}\right)^{2/3}} \right\} \end{aligned} \tag{20}$$

with $\alpha = \overline{A}\sqrt{\theta} + \theta$, $\vartheta = -\sqrt{\theta} - \overline{A}$ and $\theta = \overline{A}^2 + 4\overline{B}$. The velocity profile of Eq. (18) is valid for the whole range of parameters of the viscoelastic fluid and Newtonian solvent, i.e., it is not limited to the condition $\beta^3\epsilon De_\kappa^2 \le 2/27$ as in Afonso et al. [4], because in this case we do not use hypergeometric functions.

The normalized volumetric flow rate and the streaming electrical current (per unit of width) of the channel, can be determined from numerical integration of the velocity profile, through Eqs. (21) and (22).

$$\bar{Q} = \frac{Q}{2Hu_{sh}} = \int_{-1}^{1}\overline{u}(\overline{y})d\overline{y} = 2\int_{0}^{1}\overline{u}(\overline{y})d\overline{y} \tag{21}$$

$$\bar{I} = \frac{IH^2}{\epsilon\zeta_0 u_{sh}} = 2\int_0^1 \overline{u}(\overline{y})\overline{\kappa}^2\left(\frac{\cosh(\overline{\kappa}\,\overline{y})}{\cosh(\overline{\kappa})}\right)d\overline{y} \tag{22}$$

were by definition $I = 2\int_0^1 u(y)\rho_e(y)dy$.

For steady fully-developed channel and microchannel flows there is similarity between the solutions for the PTT and the FENE-P models as found by Oliveira [10]. Hence, this analytical solution also applies to the flow of FENE-P fluids provided some simple mathematical transformations are used as indicated in [10,11].

3. Results and discussion

In deriving the analytical solution we assumed $\overline{\varphi} = \sinh(\overline{\kappa}\,\overline{y}) \approx \frac{1}{2}\exp(\overline{\kappa}\,\overline{y}) - \frac{1}{2}$ and to study its validity, the analytical velocity profile will now be compared with the solution obtained through numerical integration of Eq. (16).

It can be easily seen that the velocity $\overline{u}(\overline{y})$, with $0 \le \overline{y} \le 1$, is given by:

$$\overline{u}(\overline{y}) = -\int_{\overline{y}}^{1}\overline{\tau}^{p}_{xy} + \overline{\kappa}\frac{\sinh(\overline{\kappa}\,\overline{y})}{\cosh(\overline{\kappa})}d\overline{y}. \tag{23}$$

This integral can be approximated using, for example, Simpson's rule. If the domain is discretized into n (even number) equally spaced panels we obtain $n+1$ grid points where the grid spacing is $h = (1-\overline{y}_p)/n$. The approximation to the integral then becomes,

$$\overline{u}(\overline{y}_p) \simeq -\frac{h}{3}\left[f(\overline{y}_0) + 2\sum_{j=1}^{\frac{n}{2}-1} f(\overline{y}_{2j}) + 4\sum_{j=1}^{\frac{n}{2}} f(\overline{y}_{2j-1}) + f(\overline{y}_n)\right], \tag{24}$$

with $\overline{y}_0 = \overline{y}_p$ and $\overline{y}_n = 1$ being the limits of integration, and $f(\overline{y}) = -\overline{\tau}^{p}_{xy} - \overline{\kappa}\frac{\sinh(\overline{\kappa}\,\overline{y})}{\cosh(\overline{\kappa})}$. The error committed by the composite Simpson's rule is bounded by

$$\frac{h^4}{180}(b-a)\max_{\xi\in[\overline{y},1]}|f^{(4)}(\xi)|. \tag{25}$$

The validity of the analytical velocity profile is tested as the influence of the solvent viscosity is assessed through the comparison between lines (analytical) and symbols (numerical). Note that the formulas obtained for the normalized shear and normal stresses are exact and do not depend on any approximation.

In the previous sections we derived the equations governing the steady fully developed EO flow of viscoelastic fluids in microchannels, taking into account the effect of the solvent viscosity. To better understand the corresponding flow dynamics, these equations are now presented via some plots by varying the different parameters involved.

We start by looking at Fig. 2 that shows the effects of the elasticity parameter ϵDe_κ^2, and of the ratio of viscosities β, on the dimensionless velocity profiles for pure electro-osmotic flow. As shown before by Dhinakaran et al. [2] the width of the EDL decreases as $\overline{\kappa}$ increases and the velocity profile becomes sharper near the wall. In the present solution the Debye-Hückel approximation is invoked, which requires $\overline{\kappa} \geqslant 10$, and in all plots we consider $\overline{\kappa} = 20$.

We observe the reduction of the normalized velocity profiles as the ratio of viscosities is decreased (increase of the polymeric concentration), consequence of the normalization of the Helmholtz–Smoluchowski velocity, which is based exclusively on the solvent viscosity. This type of behavior was also reported by Cruz et al. [11], where two different normalizations had been applied to the velocity profiles obtained by analytic solution for fully developed pressure driven laminar pipe flow of PTT fluids with different solvent ratios. They reported two different outcomes: (1) a decrease of the velocity profile normalized by the average velocity as β decreases, similar to our results in Fig. 2(a), and (2) an increase of the velocity profile normalized by the Newtonian velocity based in pressure drop and total zero shear viscosity. As we increase ϵDe_κ^2 there is an increase of the dimensionless velocity, which is more intense for intermediate values of β at $\epsilon De_\kappa^2 = 16$. This effect is better seen in Fig. 2(b), where we represent the maximum dimensionless velocity (velocity in the axis) vs. ϵDe_κ^2 for different viscosity ratios. Note that in this pure shear flow the coefficient ϵDe_κ^2 quantifies not only the elasticity via the normal stresses, but measures the shear-thinning of the viscosity that directly affects the velocity profile. An increase of the maximum velocity can be observed as we increase the ratio of the viscosities as well as the fluid shear-thinning. At large ϵDe_κ^2, the ratio $(u/u_{sh})_{\max}$ approaches a constant value (plateau), that is achieved more

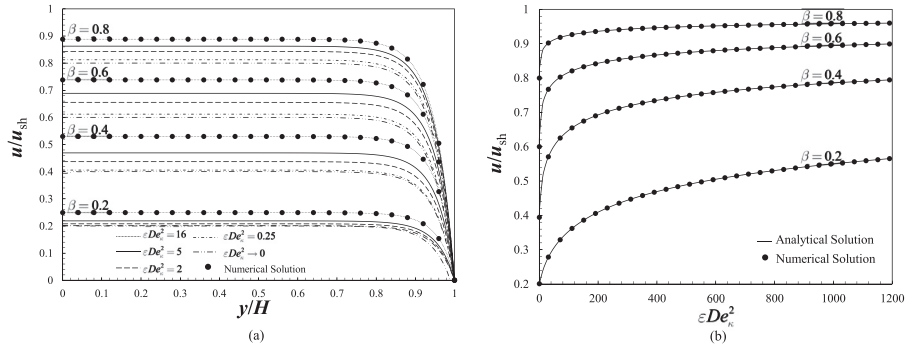

Fig. 2. (a) Dimensionless velocity profiles for viscoelastic fluid as function of ϵDe_κ^2 for several viscosity ratios, β, and $\bar{\kappa} = 20$. (b) Maximum centerline velocity as function of ϵDe_κ^2 for various viscosity ratios, β, and $\bar{\kappa} = 20$. Symbols: numerical results.

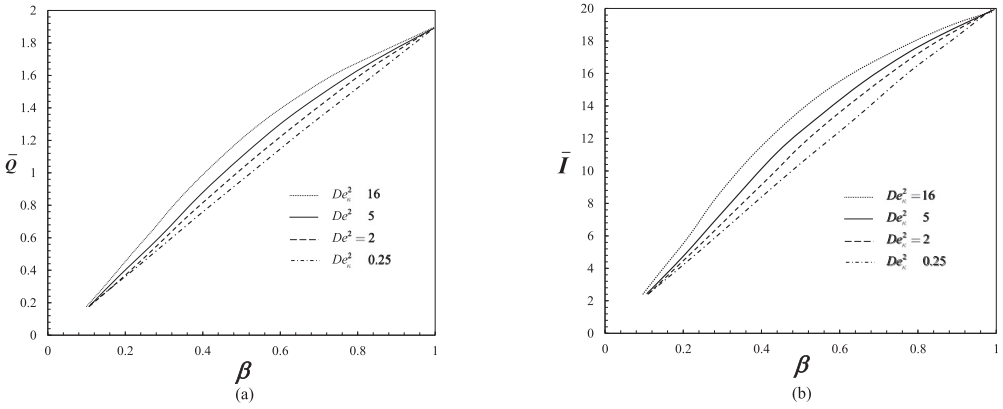

Fig. 3. (a) Dimensionless flow rate for viscoelastic fluid as function of ϵDe_κ^2 for several viscosity ratios, β, and $\bar{\kappa} = 20$. (b) Dimensionless streaming electrical current for viscoelastic fluid as function of ϵDe_κ^2 for several viscosity ratios, β, and $\bar{\kappa} = 20$. Note that due to the definition of the Helmholtz–Smoluchowski electro-osmotic velocity both quantities go to zero with decreasing β.

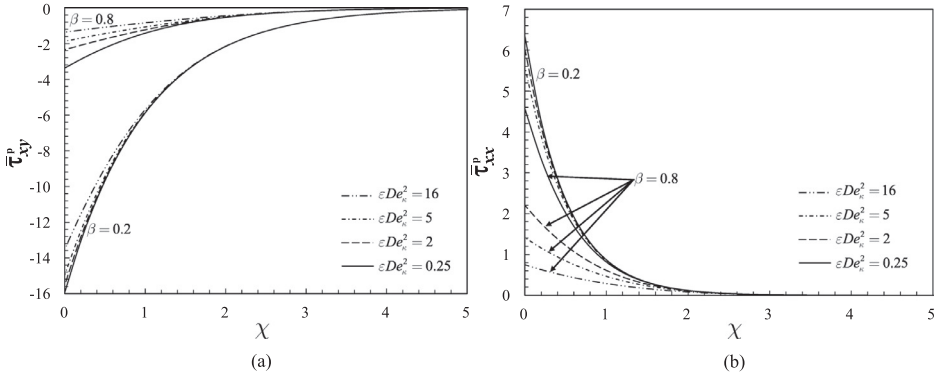

Fig. 4. Dimensionless polymeric stress profiles along $\chi = (1 - \bar{y})\bar{\kappa}$ for different values of ϵDe_κ^2 and β ($\bar{\kappa} = 20$): (a) shear stress and (b) normal stress.

rapidly for higher values of β. However for lower values of β it is possible to see a delay of this effect, with the case of $\beta = 0.2$ showing an increasing in center plane velocity.

As expected, there is a very good agreement between the analytical and numerical solutions Fig. 2(a) and (b). We have considered different values of ϵDe_κ^2 and β.

The normalized flow rate can be visualized in Fig. 3(a), where the combination of both the effect of ϵDe_κ^2 and of the solvent ratio is presented. Care should taken when analysing these results since due to the normalization adopted and the definition of u_{sh}, we obtain that $u_{sh} \to \infty$ as $\beta \to 0$. If this is not taken into account when analyzing Fig 3(a) and (b), one can wrongly infer that, for example, the flow rate goes to zero as we decrease β.

By looking at Fig. 3(a) we see that for lower ϵDe_κ^2 numbers, $\epsilon De_\kappa^2 = 0.25$, the flow rate decreases linearly with the reduction of β, and as we increase the ϵDe_κ^2 numbers the effect becomes non-linear, showing clearly an increase of the flow rate for the same solvent ratio. Another important aspect is the saturation effect of the polymeric concentration, i.e., as we reduce β the different evolutions of the flow rate for the various ϵDe_κ^2 numbers converge to the same flow rate, reducing drastically the elastic impact, where at the limit for $\beta = 0.1$ the impact of the De numbers becomes negligible. The streaming electrical current, I, normalized by $\frac{\epsilon\xi u_{sh}}{H^2}$, also calculated through numerical integration of Eq. (22) by Simpson's rule, is present in Fig. 3(b), showing similar evolution of the normalized flow rate, in terms of solvent viscosity and ϵDe_κ^2 variations, achieving the same saturation effect for $\beta = 0.1$.

Fig. 4 shows the profiles of shear and normal stresses as function of the near wall variable, $\chi = (1-\bar{y})\kappa$, for different values of ϵDe_κ^2, drawn based on Eqs. (14) and (15). We can see in Fig. 4(a) that the shear stress approaches zero away from the wall (for $\chi \geq 5$) for all values of ϵDe_κ^2 and increases rapidly near the wall, being more intense for lower values ϵDe_κ^2 and higher values of β. The saturation effect is also observed at lower values of β were the elastic contribution has a low impact, this can be observed for $\beta = 0.2$, where the shear stress profiles practically coincide for the all range of ϵDe_κ^2 presented.

The results obtained for the normal stress are qualitatively similar to the ones obtained for the shear stress, with the difference that the normal stress is positive (Fig. 4(b)). Note that a relationship between shear and normal stresses was established by Eq. (14), and therefore, as we approach to the wall the normal stress increases with more intensity for lower ϵDe_κ^2 numbers and higher values of solvent ratio.

Acknowledgements

P. R. Resende is grateful to FAPESP - Fundação de Amparo à Pesquisa do Estado de São Paulo for grant Project No. 2015/26842-3. L.L. Ferrás would also like to thank FCT for financial support through the scholarship SFRH/BPD/100353/2014. A.M. Afonso and F.T. Pinho acknowledge the support by CEFT (Centro de Estudos de Fenómenos de Transporte) and the funding by FCT (Fundação para a Ciência e a Tecnologia) through Projects PTDC/EMS-ENE/3362/2014 and PTDC/EMS-ENE/2390/2014.

References

[1] J.J. Sousa, A.M. Afonso, F.T. Pinho, Effect of the skimming layer on electro-osmotic-Poiseuille flows of viscoelastic fluids, Microfluid Nanofluid 10 (2011) 107–122.
[2] S. Dhinakaran, A.M. Afonso, M.A. Alves, F.T. Pinho, Steady viscoelastic fluid flow between parallel plates under electro-osmotic forces: Phan-thien-tanner model, J. Colloid Interface Sci. 344 (2010) 513–520.
[3] L.L. Ferrás, A.M. Afonso, M.A. Alves, J.M. Nóbrega, F.T. Pinho, Electro-osmotic and pressure-driven flow of viscoelastic fluids in microchannels: Analytical and semi-analytical solutions, Phys. Fluids 28 (2016) 093102.
[4] A.M. Afonso, F.T. Pinho, M.A. Alves, Electro-osmosis of viscoelastic fluids and prediction of electro-elastic flow instabilities in a cross slot using a finite-volume method, J. Non-Newton. Fluid Mech. 179 (2012) 55–68.
[5] M.L. Olivares, L. Vera-Candiotti, C.L.A. Berli, The EOF of polymer solutions, Electrophoresis 30 (2009) 921–929.
[6] C.L.A. Berli, M.L. Olivares, Electrokinetic flow of non-newtonian fluids in microchannels, J. Colloid Interface Sci. 320 (2008) 582–589.
[7] N. Phan-Thien, R.I. Tanner, New constitutive equation derived from network theory, J. Non-Newton. Fluid Mech. 2 (1977) 353–365.
[8] N. Phan-Thien, A nonlinear network viscoelastic model, J. Rheol. 22 (1978) 259–283.
[9] M. von Smoluchowski, Versuch einer mathematischen theorie der kogulationskinetic kolloid losunaen, Z. Phys. Chem. 92 (1917) 129–135.
[10] P.J. Oliveira, An exact solution for tube and slit flow of a FENE-P fluid, Acta Mech. 158 (2002) 157–167.
[11] D.O.A. Cruz, F.T. Pinho, P.J. Oliveira, Analytical solutions for fully developed laminar flow of some viscoelastic liquids with a Newtonian solvent contribution, J. Non-Newton. Fluid Mech. 132 (2005) 28–35.